Optics Diffraction and the FPE

Charles L. Rino
http://chuckrino.com/wordpress/

June 15, 2011

Abstract

This paper explores the equivalence between spherical wave and plane propagators. Spherical wave propagators are intrinsically part of diffraction and boundary scattering theory. However, one can construct mathematically equivalent representations of propagating waves from plane-wave superpositions. In effect, this leads to two distinctly different approaches to diffraction theory. As a practical matter, common computational methods apply when wavelength does not drive sampling requirements, which is largely confined to Fraunhofer diffraction. Fresnel scattering can lead to wavelength driven sampling, which severly limites computational methods. Examples are presented to illustrate the Fourier-domain methods.

1 Introduction

Radio frequency (RF) and optical remote sensing applications exploit diverse technologies that reflect the extreme differences in operating wavelengths. Indeed, frequency ceases to be the preferred designator of the electromagnetic wave (EM) phenomena beyond the gigahertz range. Even so, the propagation phenomena have common theoretical foundations. The essential physics is captured by the time-harmonic form of the Helmholtz equation

$$\nabla^2\psi\left(\mathbf{r}\right) + k^2\left(\mathbf{r}\right)\psi\left(\mathbf{r}\right) = 0. \tag{1}$$

The spatially varying complex wavefield, $\psi\left(\mathbf{r}\right)$, is the observable and $k\left(\mathbf{r}\right)$ is the magnitude of the local propagation vector. The practical ramifications of this common underlying phenomenology depend critically on how the extreme wavelength range influences the complexity of theoretical results that are being exploited. There is a broad class of propagation problems where wavelength does not dictate computational requirements. In that regime identical computational methods are used for RF and optics applications.

A recent development of scintillation theory as an extension of propagation theory is an example of this commonality [1]. Scintillation is caused by structure in the propagation media with gradients constrained to be small over wavelength

scales. In such *weakly inhomogeneous media* backscatter can be neglected insofar as its effects on the forward propagation from directed sources are concerned. The ensuing forward-propagation phenomena are fully characterized by a single first-order differential equation referred to as the forward propagation equation (FPE). The more familiar parabolic wave equation (PWE) is a special case of the FPE. Ray optics, in turn, is a special case of the PWE.

PWE applications are well-established in optics, RF, and acoustics. For example, consider the intensity of an optical field measured with a focal-plane array of detectors. At the resolution limit of the detectors, the intensity at each pixel is well approximated by the ray-path intensity from a source point that connects the pixel through the focal distance from the center of the array. The PWE accommodates propagation disturbances initiated by atmospheric refractive-index structure along the ray path. An antenna tracking an RF source senses ionospheric propagation disturbances along the ray path from the source to the receiver in much the same way. Although the sizes of the measurement systems and the physics that drive the constitutive relations differ considerably, the propagation model and the sampling requirements are identical.

The FPE uses a Fourier-domain plane-wave propagator, which solves (1) exactly in the absence of structure. Optics-oriented treatments of the propagation phenomena invariably start with the spherical-wave Huygens-Fresnel construction, which also solves (1) exactly in the absence of structure. The exact solutions characterize the free propagation of the source field. The theory of diffraction, which characterizes interference phenomena that develop as EM waves propagate away from their source regions, can be formulated with plane-wave propagators, although this is rarely done.

A distinction is made here between the theory of scattering, which addresses the interaction of EM waves with material objects bounded by surfaces, and the interference that results as the scattered waves propagate. A complete solution to Helmoltz equation fully captures both the median interaction and the propagation, but solutions to the Helmholtz equation that fully accommodate boundary surfaces and compact objects are not easily obtained. Indeed, the boundary-integral formulation of EM scattering theory admits no analytic solutions whatsoever.[1] Moreover, numerical solutions to the boundary-integral equations that define the source fields require sub-wavelength sampling, which severely limits practical analytic exploration.

To pursue this further, recall that Green's theorem facilitates the construction of solutions to the Helmholtz equation as superpositions of the radiation from induced sources on the boundary surfaces. Kong's development of EM boundary scattering theory, for example, is presented as the mathematical formulation of Huygen's principle. [2, Chapter 5.3] Physical optics is derived from the scalar form of Green's theorem, but the underlying phenomena is the generation of secondary EM fields initiated on boundaries and then propagated as superpositions of spherical waves.

[1] The known boundary-constrained analytic solutions to the Helmholz equation use special coordinate systems that support complete sets of basis functions that match boundary conditions intrinsically.

If, as is often the case, the boundary surfaces can be isolated by parallel planes, then propagation away from the isolating planes can be calculated by using Fourier decompositions rather than as extensions of the evolving spherical waves. The complexity of the near-field is driven in large part by the singular behavior of the Green functions, but subwavelength structure does not propagate freely. Thus, the field in a displaced boundary plane is simpler to characterize and manipulate with plane-wave decompositions. This simplification is exploited in the construction of wave-wave scattering cross sections, Fourier optics, and the FPE/PWE methodology.

This paper reviews the mathematical equivalence between plane-wave and spherical-wave propagators. The well-known Franhofer and Fresnel approximations as well as the Fourier-transform relation between a focusing lens aperture stop and the point-spread function in the focal plane are derived by using plane-wave propagators. However, as examples will demonstrate, mathematical equivalence between plane-wave and spherical-wave propagators does not imply equivalent computational demands. A rigorous test of the formal plane-wave spherical-wave propagator equivalence is the computation of the field from the aperture stop of a focusing system through the focus. As a practical matter, only the Huygens-Fresnel construction supports this calculation at optical wavelengths. The reason is the large phase curvature of the converging wavefield requires wavelength scale sampling. The Huygens-Fresnel construction has the same sampling requirement, but the computation can be localized to the small support of the focus.

2 Background

The starting point for the theoretical development is the scalar Helmholtz equation. In a medium that admits refractive index variations, the Helmholtz equation is written in the following modified form, which explicitly identifies the structure variation [1, Chapter 2]:

$$\nabla^2\psi + k^2\psi = -k^2(2\overline{\delta n} + \overline{\delta n}^2)\psi. \tag{2}$$

As noted in the introduction, $\psi(\mathbf{r})$ is the observable time-harmonic complex field. It is convenient to identify a constant mean reference background refractive index $\overline{n}$ such that $\overline{\delta n} = \delta n/\overline{n}$. It follows that

$$n = \overline{n}\left(1 + \overline{\delta n}\right). \tag{3}$$

The background refractive index is absorbed in the wavenumber definition

$$k = 2\pi f\overline{n}/c = 2\pi/\overline{\lambda}, \tag{4}$$

where f is the temporal frequency. For most scintillation applications the perturbations are small enough that the quadratic term can be ignored; moreover, the remaining occurrences of $\overline{n}$ can be replaced by unity. For example, the refractive index of the atmosphere is usually reported in refractivity units defined

as $(n-1)10^6$. However, optical glass may have a refractive index of 2 or more, which emphasizes the extreme differences in .

Equation (2.2) in Rino [1] is the vector form of (2). Equation (3-8) in Goodman[3] is the time-domain form of the parent equation that leads to (2). The derivation of the underlying modified form of the Helmholtz equation neglects the term, $\nabla(\mathbf{E}\cdot\nabla \ln n)$. *Weakly inhomogeneous media* can be defined as the class of structures for which the contribution of the gradient term is negligible. As it is applied for analysis, Equation (3-13) in Goodman [3] is equivalent to (2). The time variation of the complex fields, $\exp\{-2\pi i f t\}$, is implicit.

2.1 Boundary Integral Representations

As noted in the introduction, boundary integral representations are used to characterize the interaction of EM waves with material objects and boundary surfaces. The development in Goodman[3] follows Born and Wolf [4], which starts with the scalar boundary-integral representation

$$\psi(\mathbf{r}) = \iint\limits_{\Sigma} \left[\frac{\partial \psi(\mathbf{r}_s)}{\partial N} G(\mathbf{r}, \mathbf{r}_s) + \psi(\mathbf{r}_s) \frac{\partial G(\mathbf{r}, \mathbf{r}_s)}{\partial N} \right] ds. \tag{5}$$

In (5), $\psi(\mathbf{r})$ represents the complex field in the unbounded region outside the boundary Σ, and

$$G(\mathbf{r}, \mathbf{r}_s) = \frac{\exp\{ik|\mathbf{r}-\mathbf{r}_s|\}}{|\mathbf{r}-\mathbf{r}_s|}, \tag{6}$$

is the scalar Green function. One can show that $\psi(\mathbf{r})$ is a formal solution to Helmholtz equation by virtue of the singular behavior of the Green function as $\mathbf{r} \to \mathbf{r}_s$. The Green function and its normal derivative propagate induced fields on the boundary surfaces throughout the exterior region. A radiation condition eliminates contributions from the outer boundary that closes the Green theorem surface.

A self-consistent determination of the induced boundary fields generally requires detailed knowledge of the electric properties of the medium inside the boundary as well as the boundary surface geometry. For perfectly conducting impenetrable surfaces, the boundary integral can be manipulated as written to determine the induced fields. The ideal boundary conditions set the field or its normal derivative equal to zero on the boundary. Equations that can be solved for the unknown source fields can be obtained by taking the limit as $\mathbf{r} \to \mathbf{r}_s$, but in doing do so one must accommodate the singular behavior of the Green function and its normal derivative. However this is done, stable results demand sub-wavelength sampling.

Most practical applications of boundary-integral representations approximate the induced fields with scaled representations of the source fields. However, in the derivation of the FPE, the multiplicative interaction of the total field with the material structure permits an exact evaluation of the integral Green's theorem integral. Converting the integral equation into a pair equivalent differential equations separates the propagation and the media interaction terms.

In a homogeneous medium it can be established directly that the propagation operator satisfies the homogeneous Helmholtz equation.

For reference, the essential elements of theory of diffraction as it is developed for optical systems are captured by the Dirichlet integral representation

$$\psi(\mathbf{r}) = \iint_{\Sigma} U(\mathbf{r}_s)\, G(\mathbf{r}, \mathbf{r}_s)\, ds, \tag{7}$$

where $U(\mathbf{r}_s)$ is a source function on a representative surface. If $U(\mathbf{r}_s)$ represents an evolving spherical wavefront, (7) is a mathematical statement of the Huygens-Fresnel construction. The equivalence that will be established later is readily generalized to forms of the theory that incorporate the derivative (Neumann) term and extensions vector fields. However, the critical elements of the computation are captured by the scalar Dirichlet representation.

2.2 The Forward Approximation

The theoretical development in [1, Chapter 2] avoids an explicit treatment of scattering theory by exploiting the fact that propagating waves, however they are initiated, are highly directed if not necessarily confined to a narrow cone of scattering angles. This is made explicit by showing that (2) admits an equivalent representation as a pair of coupled first-order differential equations. The coupled equations individually characterize wave fields that propagate in opposite directions with respect to a prescribed reference axis. In the absence of the weakly inhomogeneous structure that couples the equations, the solutions are uncoupled and exact. A unidirectional source excites waves propagating in the opposite direction only through scattering interactions within the medium, but these scattering interactions are negligibly small in a weakly inhomogeneous medium.

The result is a first-order differential equation called the forward propagation equation (FPE). The following scalar FPE fully characterizes propagation in an unbounded weakly inhomogeneous medium:

$$\frac{\partial \psi(x, \varsigma)}{\partial x} = \Theta \psi(x, \varsigma) + ikS(x, \varsigma; \lambda)\, \psi(x, \varsigma). \tag{8}$$

In (8) $\psi(x, \varsigma)$ represents the complex wave field in a rectangular coordinate system with x the propagation reference axis and ς a position vector in the plane normal to the x direction, and $k = 2\pi/\lambda$ is the wave number. The source function is derived from the departure of the refractive index from unity:

$$\left(n^2 - 1\right)/2 = \delta n + \delta n^2/2, \tag{9}$$

and

$$\begin{aligned} S(x, \varsigma; \lambda) &= \delta n(x, \varsigma; \lambda) + \delta n(x, \varsigma; \lambda)^2/2 \\ &\simeq \delta n(x, \varsigma; \lambda). \end{aligned} \tag{10}$$

The leading term in (8) represents the propagation of a coherent monochromatic wave field in a homogeneous medium. The exact form of the propagation operator is

$$\Theta\psi(x,\varsigma) = \iint \widehat{\psi}(x_0,\kappa)\exp\{\pm ikg(\kappa)(x-x_0)\} \times \exp\{i\kappa\cdot\varsigma\}\frac{d\kappa}{(2\pi)^2}. \tag{11}$$

The complex field, $\widehat{\psi}(x_0,\kappa)$, is the two-dimensional Fourier transform of the field in the plane at $x = x_0$

$$\widehat{\psi}(x_0,\kappa) = \iint \psi(x_0,\varsigma)\exp\{-i\kappa\cdot\varsigma\}\,d\varsigma, \tag{12}$$

and

$$g(\kappa) = \begin{cases} \sqrt{1-(\kappa/k)^2} & \text{for } \kappa \le k \\ i\sqrt{(\kappa/k)^2-1} & \text{for } \kappa > k \end{cases}. \tag{13}$$

Irrespective of how the FPE was derived, one can readily verify by direct substitution that (11) satisfies (2) when $\delta n = 0$. Thus, solutions to the FPE in a homogeneous medium are exact solutions to the homogeneous Helmholtz equation. The unnumbered equation in Section 3.10.4 of Goodman [3] is equivalent to (11),[2] but Goodman does not use it in subsequent developments.

2.2.1 Narrow-angle scatter

For numerical integration of the FPE, the narrow-angle approximation is neither required nor advantageous. However, the narrow-angle scatter approximation is essential for analytic computations. When the spectral content of the field $\widehat{\psi}(x_0,\kappa)$ is well contained within the disk defined by $\kappa = k$, one can use the approximation

$$g(\kappa) \cong 1 - (\kappa/k)^2/2. \tag{14}$$

The Formal equivalence of multiplication in the Fourier domain by powers of κ and derivatives of the same order in the spatial domain leads to the following formal definition of the diffraction-operator and the parabolic approximation:

$$\begin{aligned} ik\Theta &= ik\sqrt{1+\nabla_\perp/k^2} \\ &\cong ik + i\nabla_\perp/(2k). \end{aligned} \tag{15}$$

The parabolic approximation (8), namely

$$\frac{\partial U(x,\varsigma)}{\partial x} = i\nabla_\perp U(x,\varsigma)/2k + ik\delta n(x,\varsigma)U(x,\varsigma), \tag{16}$$

[2] In Rino [1] the propagator is defined in terms of spatial frequencies represented by $\kappa = [\kappa_y,\kappa_z]$ where $\kappa_y = 2\pi/L$ rather than spatial frequencies.

is obtained by applying (15) and performing some straightforward manipulations. The PWE solutions apply to the modified field

$$U(x,\varsigma) = \psi(x,\varsigma)\exp\{-ikx\}, \tag{17}$$

however; removal of $\exp\{-ikx\}$ in the FPE does not influence computational requirements.

2.3 Ray Optics

The theory of ray optics is derived by approximating vector fields by products of the form $\mathbf{A}(x,\varsigma)\exp\{ik\phi(x,\varsigma)\}$. The refractive index is treated as a continuous variable. When the refractive index gradients are small, which is a necessary condition for weakly inhomogeneous media, the evolving field structure can be characterized by propagation along geometric ray paths. The ray trajectories are defined by position-dependent vectors $\mathbf{r}(s)$, where s is the distance along the ray. The vector $\mathbf{r}(s)$ is constrained locally by two orthogonal vectors, namely the unit vector $\mathbf{s}$ tangent to the ray at $\mathbf{r}(s)$ and the curvature vector $\varkappa = d\mathbf{s}/ds$, which is normal to $\mathbf{s}$. The ray trajectory in the medium must satisfy the ray equation

$$n\varkappa + \frac{dn}{d\mathbf{s}}\mathbf{s} = \nabla n. \tag{18}$$

This equation can be derived from (16) by assigning the phase variation $\exp\{ik\phi(x,\varsigma)\}$ to $U(x,\varsigma)$[5, Chapter 5.2]. This is the basis for the earlier claim that ray optics in unbounded media is contained in the broader class solutions to the FPE. Note that aside from the wavelength dependence of the refractive index, the ray trajectories are wavelength independent.

2.4 Optical Lens Systems

Optical lens systems require special treatment for two reasons. First, a lens is defined by discontinuous boundaries, which often have discontinuous normal derivatives as well. Second, the diffraction effects that limit the resolution of optical systems ultimately must be incorporated into the analyses. A highly simplified lens system is used here to illustrate the use of ray optics to approximate a starting field for Fourier-domain computation.

Consider a representative lens system constructed from a colinear arrangement of homogeneous radially symmetric lens objects. For simplicity, lens objects will be confined to closed volumes circumscribed by intersecting spherical segments. As already noted, boundary scattering theory tells us that the transmission and scattering (reflecting) properties of lens objects are determined by the shape of the defining boundary surfaces and the constitutive properties of the lens material. The dielectric properties are defined by a frequency-dependent refractive index. From ray theory it follows that ray paths within homogeneous lens objects are straight lines.[3]

[3]For this development only monochromatic radiation will be considered.

A planar boundary admits an exact solution that can be constructed by applying Snell's law to determine the wavefront propagation directions on either side of the boundary:

$$\frac{\sin\theta_1}{\sin\theta_2} = \frac{n_2}{n_1}. \tag{19}$$

If the boundary variations are smooth enough, the boundary conditions are approximated by applying Snell's law with respect to the surface normal. The implicit assumption here is that the lens system is sufficiently uniform that rays can be approximated by straight lines inside lens objects. Thus, ray segments can be defined by unit vectors, $\mathbf{u}_i$, where i corresponds to the side of the boundary in which the ray is defined. Let $\mathbf{u}_n$ represent a unit vector normal to the surface. At the boundary

$$\mathbf{u}_i \cdot \mathbf{u}_n = \cos\theta_1,$$

which defines $\sin\theta_1$. Snell's law defines $\sin\theta_2$, which is measured with respect to $-\mathbf{u}_n$. The following pair of equations define the continuation of ray trajectories within lens objects:

$$-\mathbf{u}_n \cdot \mathbf{u}_2 = \sqrt{1-\sin^2\theta_2} \tag{20}$$

$$-\mathbf{u}_n \times \mathbf{u}_2 = \sin\theta_2 \tag{21}$$

Knowing $\mathbf{u}_2$, one can calculate the intersection of the ray with the opposite lens cap. The process can then be repeated to determine the direction of the rays exiting the lens object. There are many utilities available that will perform completely general ray analyses of lens systems and report the results graphically or in tabular form. However, the simpler formulation is useful for illustrative purposes. Figure 1 shows the evolution of a bundle of paraxial rays through a bispherical lens. The cap radii are 120 mm. The lens thickness is 10 mm. The refractive index at .46 μ is 1.62. The red pentagram show the nominal location of the focus calculated from the lens equation

$$\frac{1}{f} = (n-1)\left(\frac{1}{r_1} - \frac{1}{r_2} + \frac{(n-1)}{n}\frac{d}{r_1 r_2}\right), \tag{22}$$

where $\pm r_n$ is the positive convex radius of curvature of the lens faces, and d is the thickness of the lens along the central ray.

2.4.1 Field Estimation

The modified ray-optics construction just described is the only practical way to compute an optical field in the aperture stop of a lens system. Consider the normal plane at $x = 10$ mm. The optical path is defined as the ray-path integral weighted by the refractive index:

$$s = \oint n ds = \sum_i n_i s_i. \tag{23}$$

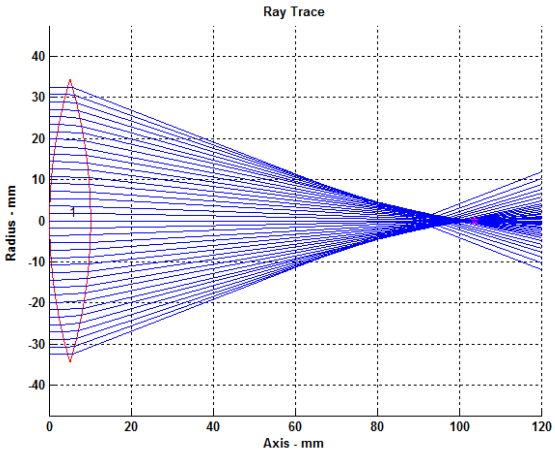

Figure 1: Vertical cross section of the ray-trace evolution of a parallel bundle of rays interacting with a bispherical lens. The red pentagram shows the predicted focal point.

The summation is over the three straight-line paths that connect points in the entrance plane to points in the exit plane. The complex field in the vertical plane has the form

$$\psi\left(x,\varsigma'\right)=A\left(x,\varsigma'\right)\exp\left\{iks(\varsigma')\right\}. \tag{24}$$

The amplitude weighting accounts for the increased field intensity necessary to conserve energy as the field intensity becomes more concentrated, but that small correction will be ignored here. Figure 2 shows the optical path computed at the exit plane of the lens object shown in Figure 1. An eighth-order polynomial fit was used to approximate the optical path.

Figure (3) shows the difference between a purely quadratic phase variation and the phase variation deduced from ray-optics for the bispherical lens. It can be see that the departures become more pronounced as the edges of the lens are approached. In effect the resolving power of the lens implied by its diameter cannot be realized.

2.5 Forward Propagation

This section presents a development of what is usually referred to as the theory of diffraction by using only the plane-wave propagator. The formal equivalence between the formal equivalence between the Huygens-Fresnel integral representation and the FPE are also demonstrated. The standard developments use the narrow-angle scatter approximation, whereas the Fourier-domain propagator can be applied without constraint. However, the examples show that

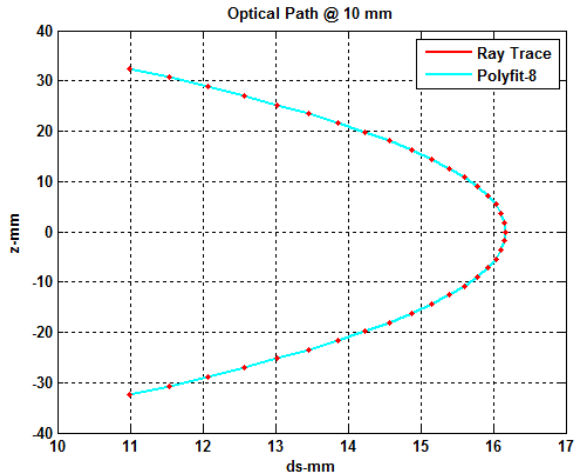

Figure 2: Optical path length computed from ray-trace (red dots) . Cuyan curve is least-squares fit to 8th order polynomial.

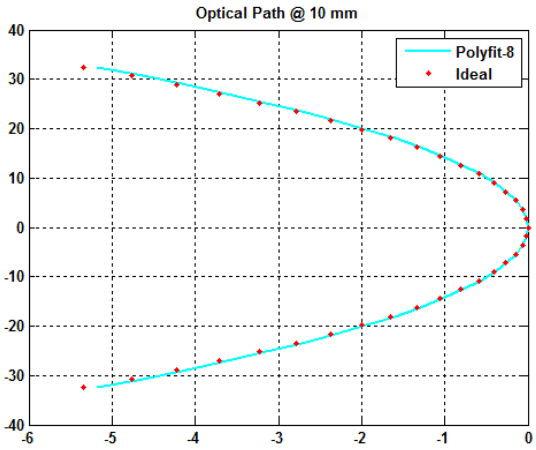

Figure 3: Ideal phase correction to produce a focus at a distance f from the aperture plane.

wavefront curvature imposes severe computational requirements. Although Huygens-Fresnel requires the same sample density, it allows localization of the computation. For this reason Huygens-Fresnel is the only viable construct for calculating diffraction effects at optical wavelengths for high-curvature wavefields.

2.5.1 Full-Wave Diffraction

In an unobstructed homogeneous region, the solution to the scalar Helmholtz equation is determined by the field in the plane at $x = x_0$, which will be referred to as the aperture plane. If the actual aperture plane is tilted, a linear phase variation can be applied to launch the wavefield normal to the orientation of the computation plane [6]. Alternatively, the propagator itself can be written for evaluation along the principal propagation direction [1, Chapter 4]. However, for the purposes of the development here these details are unimportant.

If one is interested in the field only at a large distance from the aperture plane, the solution takes a particularly simple form. An application of the stationary phase approximation to (11) will show that

$$\lim_{\Delta x \to \infty} \Theta\psi\left(\Delta x, \varsigma\right) = -ig(\kappa_r)\left[k^2\widehat{\psi}(0;\kappa_r)\right]\frac{\exp\{ikr\}}{2\pi kr}, \tag{25}$$

where $r = \sqrt{\Delta x + \varsigma^2}$ and κ_r is the transverse wavenumber in the direction of $\mathbf{r} = [\Delta x, \varsigma]$. It is fundamental to the design of remote sensing systems because it defines the on-axis signal intensity at distance r from the source. Off axis, the field variation is defined by the Fourier transform of the aperture distribution. In optics literature, (25) is called Fraunhofer approximation [3, Chapter 4]. Although the narrow-angle scatter approximation was not used in the derivation presented here, narrow-angle scattering is implicit because the transverse dimensions are necessarily small when $\Delta x \to \infty$.

The near-field is a much more demanding environment. To explore the near field, it is convenient to rewrite (11) as an explicit linear operation on the starting field:

$$\begin{aligned}\Theta\psi\left(x, \varsigma\right) = \iint \left[\iint \psi\left(x_0, \gamma/k\right)\exp\left\{-i\eta\cdot\gamma\right\}d\gamma\right] \\ \times \exp\left\{i\sqrt{1-\eta^2}\left(k\Delta x\right)\right\}\exp\left\{i\eta\cdot k\varsigma\right\}\frac{d\eta}{\left(2\pi\right)^2}.\end{aligned} \tag{26}$$

Changing the order of integration isolates the singular inner integral:

$$\begin{aligned}\Theta\psi\left(x, \varsigma\right) \approx \iint \psi\left(x_0, \gamma/k\right) \\ \times \left[\iint \exp\left\{i\sqrt{1-\eta^2}\left(k\Delta x\right)\right\}\exp\left\{i\eta\cdot\left(\left(k\varsigma\right)-\gamma\right)\right\}\frac{d\eta}{\left(2\pi\right)^2}\right]d\gamma,\end{aligned} \tag{27}$$

However, the exchange is justified when the spectral content of the starting field is limited to a narrow range of propagation angles, say where $\sqrt{1-\eta^2} \simeq 1-\eta^2/2$. It then follows that

$$\Theta\psi\left(x,\varsigma\right) \simeq \exp\left\{ik\Delta x\right\} \iint \psi\left(x_0,\gamma/k\right) \times \iint \exp\left\{-i\eta^2\left(k\Delta x/2\right)\right\} \exp\left\{i\eta\cdot\left(\left(k\varsigma\right)-\gamma\right)\right\} \frac{d\eta}{\left(2\pi\right)^2} d\gamma. \tag{28}$$

The Fourier transform represented by the η integration can be evaluated analytically. Carrying out the integration leads to the following near-field form of the equation, which is called the Fresnel approximation

$$\begin{aligned} \Theta\psi\left(\Delta x,\varsigma\right) &\simeq \frac{-ik\exp\left\{ik\Delta x\right\}}{2\Delta x} \\ &\times \iint \psi\left(0,\varsigma''\right) \exp\left\{i\left(\varsigma-\varsigma\right)^2 k/\left(2\Delta x\right)\right\} d\varsigma'' \qquad (29) \\ &= \frac{-ik\exp\left\{ik\Delta x\right\}}{2\Delta x} \exp\left\{i{\varsigma}^2 k/\left(2\Delta x\right)\right\} \\ &\times \iint \left[\psi\left(0,\varsigma''\right) \exp\left\{i{\varsigma''}^2 k/\left(2\Delta x\right)\right\}\right] \exp\left\{-i\varsigma.\varsigma''\left(k/\Delta x\right)\right\} d\varsigma'', \qquad (30) \end{aligned}$$

The two forms of the result are identical to Goodman's Equations (4-14) and (4-17). The fact that the final form of the Fresnel approximation is itself a Fourier transformation should not be confused with the Fourier transformation in the propagation integral (26), which involves no approximations.

The reason for rederiving these well know results here is to show that they are special cases of full wave propagation, which can be evaluated numerically by using Fourier transformations. Moreover, there is no compelling reason to impose the narrow scatter approximation if numerical computation is being pursued. For the Fraunhofer regime, this is empty generality because there are few, if any, practical situations where the narrow-angle scatter approximation is violated. This is manifestly not the case in the Fresnel region. To explore this, consider the Huygens-Fresnel construction, which is also exact insofar as the propagation of a known starting field is concerned. The main difference is that the Huygens-Fresnel starting field is defined on a surface that need not be planar.

Starting with Huygens-Fresnel, consider the field in a plane at $x = x_0$ that isolates the defining surface from an unobstructed propagation space. From (7),

$$\psi_{HF}\left(x_0,\varsigma\right) = \iint_{\Sigma} U\left(\mathbf{r}_s\right) \frac{\exp\left\{ik\left|x_0-x_s,\varsigma-\varsigma_s\right|\right\}}{\left|x_0-x_s,\varsigma-\varsigma_s\right|} ds. \tag{31}$$

Substituting the Weil representation of the Green function,

$$\frac{\exp\{ik\,|\Delta x, \varsigma - \varsigma'|\}}{|\Delta x, \varsigma - \varsigma'|} = \iint \frac{i\exp\{ikg(\kappa)\Delta x\}}{2kg(\kappa)} \exp\{i\kappa\cdot(\varsigma - \varsigma')\}\ \frac{d\kappa}{(2\pi)^2}, \quad (32)$$

into (31) and reversing the order of integration as before shows that

$$\begin{aligned}\psi_{HF}(x,\varsigma) &= \iint_{\Sigma} U(\mathbf{r}_s) \iint \frac{i\exp\{ikg(\kappa)\Delta x\}}{2kg(\kappa)} \exp\{i\kappa\cdot(\varsigma - \varsigma_s)\}\ \frac{d\kappa}{(2\pi)^2} ds \\ &= \iint \left[\frac{i}{2kg(\kappa)} \iint_{\Sigma} U(\mathbf{r}_s)\exp\{-i\kappa\cdot\varsigma_s\} ds\right] \exp\{i\kappa\cdot\varsigma\} \\ &\quad \times \exp\{ikg(\kappa)\Delta x\}\ \frac{d\kappa}{(2\pi)^2}. \end{aligned} \quad (33)$$

Evaluating the two-dimensional Fourier transform of $\psi_{HF}(x_0,\varsigma)$[4] establishes the equivalence

$$\widehat{\psi}_{HF}(x_0,\kappa) = \frac{i}{2kg(\kappa)} \iint_{\Sigma} U(\mathbf{r}_s)\exp\{-i\kappa\cdot\varsigma_s\} ds. \quad (34)$$

Rewriting (33) in terms of $\widehat{\psi}_{HF}(x_0,\kappa)$ reproduces the plane-wave propagator:

$$\psi_{HF}(x,\varsigma) = \iint \widehat{\psi}_{HF}(x_0,\kappa)\exp\{ikg(\kappa)\Delta x\}\ \frac{d\kappa}{(2\pi)^2}. \quad (35)$$

Note that (34) defines the Fourier transformation as an integration over the induced sources of the field. It shows as well that the subsequent propagation of that field can be calculated in principle without approximation using Fourier-domain methods.

However, the factor $1/g(\kappa)$ in (34) is singular at $k = \kappa$. For $k < \kappa$ it has little effect; moreover, to properly accommodate the singularity requires careful evaluation. The poles in the spatial Fourier domain are necessary for generating the singular behavior of the Green function. With the singular points in the source region well removed from the plane at $x = x_0$, this term can be safely ignored.

Reciprocity provides another example of the equivalence between Green-function and plane-wave representations. The Green function is intrinsically symmetric to an interchange of the source and field point variables, which leads to the reciprocal interchange between a source point and a measurement point. It is also true that a spectral domain representation that maps incident plane waves to forward or scattered plane waves can be constructed for invariance to an interchange of wave vectors. [7].

[4] $\Delta x = 0 \Leftarrow x = x_0$

3 Numerical Examples

There are two integral representations of a propagator that can be used for computing the free-space evolution of a starting field. To the extent that the computation is to be done numerically, sampling requirements dictate the most efficient method. If the split-step Fourier-domain method is used to solve the FPE, there is no compelling reason to approximate the propagation operator. If finite-difference methods are used, the diffraction operator must be approximated. This can be advantageous if the spatial-domain support of the field constrained. In any case, it is the Fresnel region that is most demanding.

3.0.2 Fraunhofer Diffraction

The first example uses a zero-phase starting field defined in a plane. A uniform circular "top hat" is a convenient realization because it admits an exact transform:

$$\begin{aligned}\widehat{\psi}\left(x_0,\kappa\right) &= \iint\limits_{-D/2}^{D/2} \exp\left\{-i\zeta\cdot\kappa\right\} d\zeta \\ &= \int\limits_0^D \zeta \int\limits_0^{2\pi} \exp\left\{-i\kappa\zeta\cos\phi\right\} d\phi d\zeta \\ &= \frac{2\pi}{\kappa^2}\int\limits_0^{\kappa D} \eta J_0\left(\eta\right) d\eta = \frac{2\pi D}{\kappa} J_1\left(\kappa D\right). \end{aligned} \tag{36}$$

From (30), the field in the focal plane of a lens is

$$\psi\left(f,\varsigma\right) \sim \frac{2\pi f D}{k\varsigma} J_1\left(k\varsigma D/f\right).$$

The standard estimate of the focal spot size

$$d = 1.22\lambda f/D, \tag{37}$$

follows [3, Equation (4-32)].

Consider a uniform circular 0.46 μ source with diameter $D = 68.56$ mm, which is the maximum extent of the lens used in the ray-trace example. Standard discrete Fourier transform (DFT) sampling requirements establish the relation

$$\Delta L \Delta K = \frac{2\pi}{N}.$$

Since the power-spectrum of the complex wavefield is invariant to propagation, the source field determines the sampling interval. In the far-field the beam will expand at a rate dictated by the angular extent of the Fourier-transform of the disc normalized to wavenumber. Since the expanding beam must stay

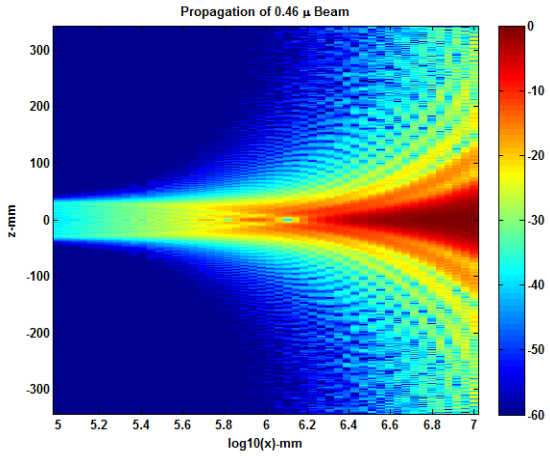

Figure 4: FPE computation of the forward propagation of an unfocused circular spot. The field intensity is a vertical slice of the two-dimensional field multiplied by the square of the propagation distance.

within the computation grid to minimize edge effects, a span of $5D$ was used to accommodate a propagation distance of 10 m. Note that although $D/\lambda = 1.5 \times 10^5$, adequate sampling was achieved on a 4096×4096 grid with $\lambda/dy = \lambda/dz = 364$.

Figure 4 shows a the vertical plane intensity for 50 logarithmically spaced propagation steps. The field has been normalized to its on-axis peak, which becomes constant when the Fraunhofer limit is achieved. Logarithmic propagation steps were used to capture the evolution from the near field to the far-field limiting form. One can verify that the sidelobes are predicted by the Fourier transform of the disk. Note that in the point-spread function in the focal plane of a lens (30) has the overall same shape.

Each computation step requires forward and inverse DFTs with in intervening matrix multiplication. The computation used approximately 20 s per step on a 64-bit, dual-processor PC with 8 GBytes of memory.

If one were interested only in free-space propagation, the computation of the far-field limit would be of academic interest. However, if the propagation medium is structured, the split-step method accommodates the effects of the structure without further approximation.

3.0.3 Fresnel Diffraction

Computation of Fresnel diffraction in the absence of high curvature are well established [3, Section 4.5]. However, Zeng and McGough did use the full-wave propagator for a low-curvature acoustics application[8]. The more challenging

application is the focusing of the wave field as it propagates from the plane of a lens system aperture stop. Although ray-optics could be used to estimate the focal plane field, the simpler top-hat form with an appropriate phase variation will be used here. The spherical wave to aperture distance might be used as a surrogate:

$$\psi(\zeta) = \exp\left\{ikf\left(1 - \sqrt{1 - \zeta^2/f^2}\right)\right\} \text{ for } \zeta < D/2. \tag{38}$$

On the other hand, the Fresnel approximation shows that an aperture distribution with quadratic phase, namely

$$\psi(\zeta) = \exp\left\{ik\zeta^2/(2f)\right\} \text{ for } \zeta < D/2, \tag{39}$$

is consistent with the Fourier-transform relation between the uniform aperture and the focal-plane PSF. The aperture fields (38) and (39) are nearly equal for large f/D ratios.

Sampling requirements are driven by the extreme phase variation at optical frequencies ($k > 10^5$). It should not be surprising that near-wavelength sampling is necessary. Trial and error showed that sampled fields similar to the Fraunhofer example could be used only for wavelengths in the millimeter range. The focal length and aperture size were adjusted to provide a large aperture in wavelengths.

To demonstrate the sampling requirements, Figure 5 shows the focal-plane spectral density plotted against wavenumber normalized by k. An aperture diameter of 60 mm was used with $k = 10$ reciprocal millimeters ($f = 477.5$ GHz). The quadratic source field defined by (39) with $f = 140$ mm was used. The computation shows that the significant portion of the spectral intensity occupies nearly 50% of the range of non-evanescent waves, which is well beyond narrow-angle scatter limits. In effect, the sample spacing must resolve π radian phase changes.

With adequate sampling, the field in any forward plane can be computed by applying the Fourier-domain propagator. Figure **??** shows a vertical-plane cut of the field intensity computed over 111 planes centered on the nominal focal distance with 1-mm spacing. The x distance is measured from the exit plane, which accounts for the displacement of the focus from 140 mm. Figure 6 shows the detail of the Focal plane intensity. It is imperceptibly different from the scaled Fourier transform of the Fourier-transform of the aperture stop as predicted by (30).

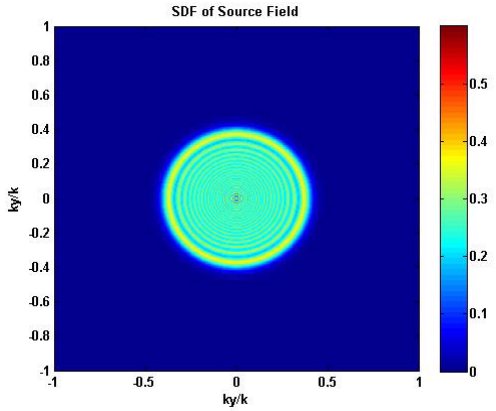

Figure 5: Spectral density function plotted against normalized spatial wavenumber for qadratic-phase starting field.

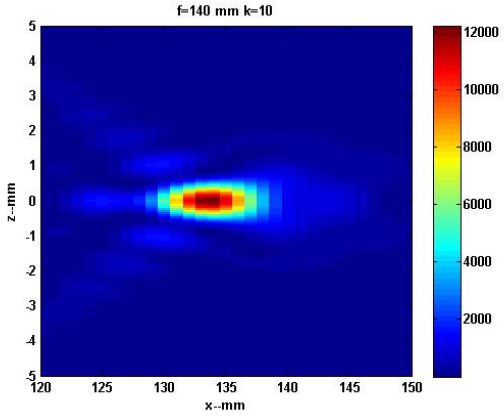

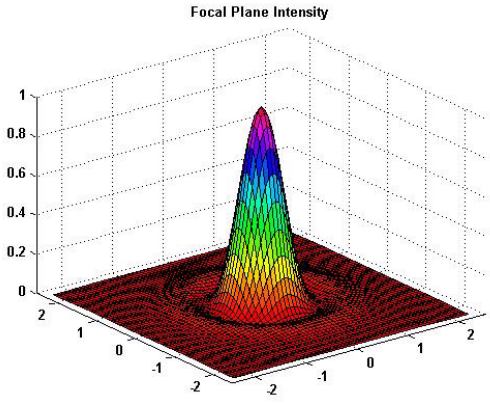

Figure 6: Focal plane field intensity.

Acknowledgement

The assistance of Dennis Hancock in clarifying concepts and optical methodology is gratefully acknowledged. http://dennishancock.com/

References

[1] Charles L. Rino. *The Theory of Scintillation with Applications in Remote Sensing*. John Wiley and Sons, Inc., New York, 2011.

[2] J. A. Kong. *Electromagnetic Wave Theory: Second Edition*. John Wiley & Sons, New York, 1986.

[3] Joseph W. Goodman. *Introduction to Fourier Optics*. Roberts and Company, Connecut, 2005.

[4] M. Born and E. Wolf. *Principles of Optics*. Cambridge University Press, 1999.

[5] Mireille Levy. *Parabolic Equation Methods for Electromagnetic Wave Propagation*. Institute of Electrical Engineers, United Kingdom, 2000.

[6] N. Delen and B. Hooker. Verification ofn comparison of a fast fourier transform-based full diffraction method for tilted and offset planes. *Applied Optics*, 40(21):3525–3531, 2001.

[7] Hoc D. Ngo and Charles L. Rino. Wave scattering functions and their application to multiple scattering problems. *Waves in Random Media*, 3(3):199–210, 1993.

[8] Xiaozheng Zeng and Robert J. McGough. Evaluation of the angular spectrum approach for simulations of near-field pressures. *J. Acoust. Soc. Am.*, 123(1):68–76, 2008.